# Model-Based Analysis and Evaluation of an Origami Encounter-type Wearable Device

Monica Malvezzi, Lisheng Kuang, Claudio Pacchierotti, Francesco Chinello

# Model-Based Analysis and Evaluation of an Origami Encounter-type Wearable Device

Monica Malvezzi[1], Lisheng Kuang[2], Claudio Pacchierotti[2], and Francesco Chinello[3]

***Abstract*— This paper presents the analysis of an origami-inspired wearable haptic device designed for cutaneous interaction with the palm. The device employs a structured mechanism to render edges, tips, and surfaces by dynamically adjusting force and velocity parameters. A detailed evaluation of inverse kinematics and velocity-force relationships is conducted to evaluate device reachable configurations and performance in trajectory execution. The findings contribute to the development of advanced wearable haptic systems, improving tactile interaction and enhancing user experience in digital and physical applications.**

## I. Introduction

Wearable haptic technology has significantly advanced in the past years [1], [2], enhancing touch-based interactions in various applications, particularly in teleoperated scenarios where balancing stability and transparency is essential. Notable progress has been made in leveraging both cutaneous and kinesthetic feedback to improve task performance, especially through haptic cues at the fingertip level. Among the most relevant applications of wearable haptics is Virtual Reality (VR), where realistic interaction with virtual objects is crucial for immersion, presence, and task effectiveness [1], [3]–[5]. By integrating visual and tactile feedback, wearable haptic systems have opened new opportunities for enhancing material perception and user interaction in digital environments [6]. Recently, significant challenges are related to the possibility in VR or non-VR scenarios, to actually be able to provide the user a fully immersive haptic experience. The latter includes the possibility of rendering various surfaces enriched by edges, tips, or flat parts. This has a significant impact on the experience of exploring and understanding surfaces, without the need to change the available interactive device. The design of wearable haptic devices is of course closely linked to the specific body area they target. Since the skin is the body's largest organ, covering approximately two square meters and weighing around four kilograms on average [7], researchers have explored various skin regions for tactile feedback applications. These include the face and forehead [8], [9], neck [10], [11], torso [12], forearm [13], [14], shoulder [15], and legs [16]. While the fingertips remain a primary focus due to their sensitivity in exploration and grasping tasks [17], increasing attention is being given to the palm, which plays a crucial role in manipulation and interaction. Recent research has explored tactile feedback for the hand palm, aiming to enhance virtual interactions by improving softness perception [18] and developing innovative haptic interfaces for VR [19]. This study focuses on haptic feedback for the palm, an area still undergoing extensive research. Although significant progress has been made in designing devices that render pressure and vibration on the palm surface [19], representing objects' shapes through surfaces, edges, and tips remains challenging. Recent advancements, such as origami-inspired foldable structures for haptic displays [20], [21], offer promising solutions. These encounter-type haptic devices can function as both wearable tactile systems and stationary haptic platforms. In this paper, we analyze the force and velocity dynamics of origami-inspired tactile devices actuated by a 7-Degrees of Freedom (DoF) parallel robot, designed for hand palm-based interaction.

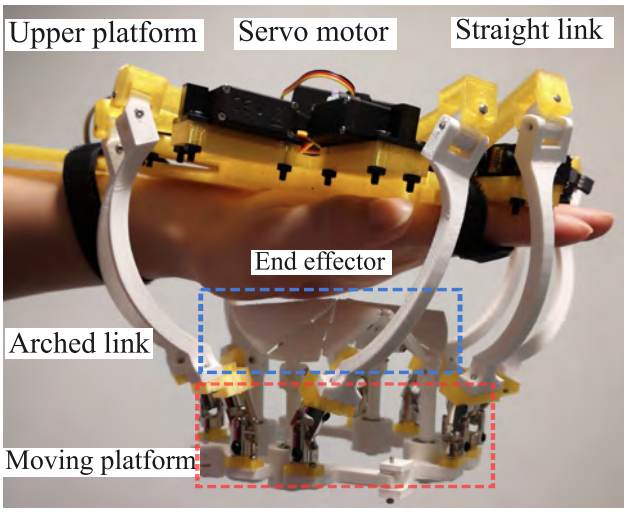


Fig. 1: The device prototype on hand. Its structure is composed of a redundant parallel robot with 7-DoF and 8-DoA, while the end-effector is an origami structure. The mechanical design of the device is open-sourced via this repository on Github: https://github.com/lisheng-kuang/7DoFHapticDevice.git.

## II. Related Work

The development of haptic devices spans a wide range of hardware solutions, each designed for specific appli-

*We acknowledge the support of the European Union by the Next Generation EU project ECS00000017 "Ecosistema dell'Innovazione" Tuscany Health Ecosystem (THE, PNRR: Spoke 9: Robotics and Automation for Health) and the European Union's Horizon Europe research and innovation programme (grant No 101070066, project REGO).

[1]M. Malvezzi is with the University of Siena (Siena, Italy) and the Istituto Italiano di Tecnologia (Genova, Italy). monica.malvezzi@unisi.it

[2]L. Kuang and C. Pacchierotti are with CNRS, Univ Rennes, Inria, IRISA (Rennes, France).

[3]F. Chinello is with Aarhus University (Herning, Denmark).

cations, case studies, mechanical advancements, or haptic stimuli. Several designs focus on wearable haptic devices that provide tactile cues at the palm level. Notable examples include LinkGlide and DeltaTouch, which deliver skin-level haptic feedback for immersive and non-immersive virtual reality (VR) applications [18], [19]. While these solutions enhance VR interactions, they do not incorporate velocity-force model characterization through simulation, limiting the control opportunities [22]. Giraud et al. [23] designed a 3-DoF wearable fingertip haptic device, called Haptigami, to deliver rich haptic feedback to the fingertip. Providing various types of feedback typically requires multiple DoF and high mechanical complexity, which are challenging to achieve at the mesoscale [23]. To address this, Haptigami employs compliant low-profile transmissions embedded in an origami structure and PCB motors as actuators. This under-actuated system, weighing 13 g, can render both vibrotactile and cutaneous haptic sensations. Villani et al. [24] proposed a wearable haptic device dedicated to the palm, initially introduced in [25]. Their design consists of a rigid structure with three servomotors pulling tensors to manipulate a tactor in contact with the palm. The study analyzed the forces exerted by the device on the skin; however, it was limited to a specific wearable device design with interchangeable tactors with a fixed structure. More recently, Iiyoshi et al. [20] introduced an origami-inspired handheld device that provides force feedback for anesthesia training. Similar designs [26] function either as handheld or desktop-based haptic devices. Additionally, Korres et al. [27] presented a flexible vibrotactile actuator inspired by origami, while Williams et al. [28] developed a 4-degree-of-freedom parallel haptic device capable of delivering normal force, shear, and torsion feedback at the fingertip level. Ren et al. [29] introduced WORM (Wearable Origami Rendering Mechanism), which employs a magnetic field to generate controllable haptic illusions. Inspired by the work of Kuang et al. [21], this paper focuses on the force and velocity analysis of an origami-based platform for tactile sensation through simulation actuated by a 7-DoF, 8-Degrees of Actuation (DoA) parallel robot with a structure in principle similar to [30]. Unlike the haptic device proposed in [30], the design presented in [21] has a smaller size can function as a wearable, desktop, or encounter-type device integrating the parallel structure with an origami-based end effector. With respect to prior work, in this paper we detail a force and velocity analysis based on simulation, offering a deeper understanding and a significant contribution to the literature on origami-inspired wearable haptic systems.

## III. Structure and Working Principle

### A. Device description

Our previous work has introduced the device mechatronics design and main characteristics [21]. While in order to provide a clear description of the device, we represent the device again in Fig. 1 and the device scheme in Fig. 2. The device is designed to manipulate an origami based end-effector that can contact the hand palm in different ways,

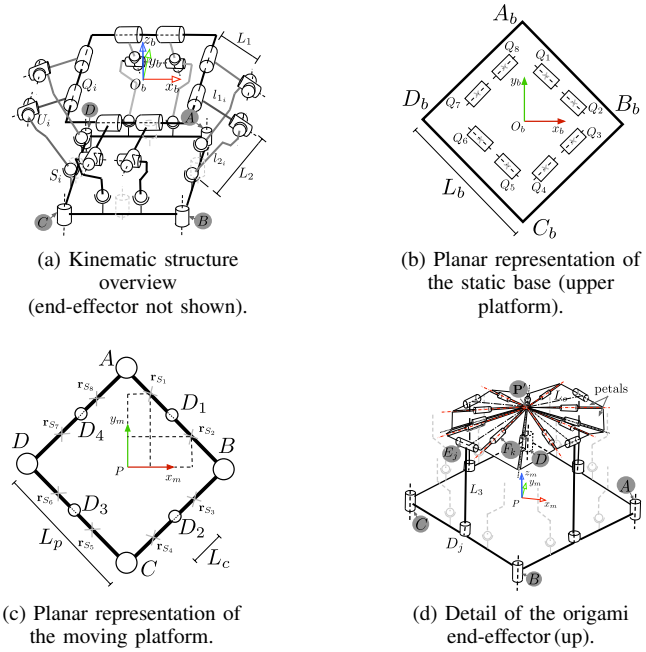


(a) Kinematic structure overview (end-effector not shown).

(b) Planar representation of the static base (upper platform).

(c) Planar representation of the moving platform.

(d) Detail of the origami end-effector (up).

Fig. 2: Device structure presented in our previous work [21], (a) the device is composed of three interconnected elements: (b) a static base to host the servo motors, (c) an articulated four-bar frame (d), an origami end effector. We recall these from our previous work to demonstrate the kinematics.

simulating the interaction with flat surfaces, edges and points. The device can be synthetically divided in two parts: the actuation unit and the end-effector. The actuation part of the device consists of a parallel robot, composed of two platforms -the base platform and the moving platform - connected by eight identical articulated legs with a RUS (Revolute-Universal-Spherical) structure, as shown in Fig. 2a. Each leg has an active revolute joint $Q_i$ connecting the base platform and with the link $l_{1,i}$ (length $L_1$), which is actuated by a servomotor screwed on the base platform.

### B. Kinematics analysis

Inverse kinematics analysis aims to define a relationship between the end-effector configuration and actuated joints' rotation angles. The analysis can be conveniently divided into two parts: the origami end effector and the actuation unit. The origami end effector configuration is defined by a 7-dimensional vector $\boldsymbol{\nu} = [x'_P, y'_P, z'_P, \alpha, \beta, \gamma, \delta]^{\mathrm{T}}$, containing the coordinates of $P'$ vertex, origami structure orientation w.r.t. the base frame $\mathcal{S}_b$, defined for example by the roll, pitch, yaw angles, $\alpha, \beta, \gamma$, and vertex's angle $\delta$, defined as the angle between the planes containing a pair of opposite active petals.

The first step of the inverse kinematic analysis consists in finding the relationship between the origami configuration $\boldsymbol{\nu}$ and the actuation unit mobile platform configuration, which can be represented by the vector $\mathbf{u}$, i.e.

$$\mathbf{u} = \mathbf{f}_{ik,o}\boldsymbol{\nu} \tag{1}$$

More specifically, the mobile platform configuration can be described by the 7-dimensional vector $\mathbf{u}$ =

$[x_P, y_P, z_P, \alpha, \beta, \gamma, \rho]^{\mathrm{T}}$ containing the coordinates of $P$ point with respect to base reference frame $\mathcal{S}_b$, orientation angles $\alpha, \beta, \gamma$ (the same of the origami structure), and the parameter $\rho$, adopted to represent the articulated diamond configuration, defined as half of the diamond diagonal aligned with $y_m$-axis. Let us indicate with $\mathbf{R}_m^b$ the rotation matrix relating the base and local reference frames, that can be evaluated as a function of $\alpha, \beta, \gamma$ angles. The coordinates of $P$ points, collected in the vector $\mathbf{r}_P$ can be evaluated as:

$$\mathbf{r}_P = \mathbf{r}'_P - \mathbf{R}_m^b \mathbf{r}_{PP'}^m \tag{2}$$

where $\mathbf{r}_{PP'}^m = [0,\ 0,\ L_3 + L_o \cos(\delta/2)]^{\mathrm{T}}$ are the coordinates of $P'$ point in the platform reference frame. Finally, the platform configuration parameter $\rho$ can be related to origami angle $\delta$ through straightforward geometrical considerations that are not detailed here for the sake of conciseness.

The spider structure can be represented as a redundant 7-DoF parallel structure actuated with 8 motors, leaving the mobile platform free from actuators. Eight links are connected to the fixed platform by revolute joints, let us indicate with $Q_i$ joint centers. Let us indicate with $\mathbf{q} = [q_1, ..., q_8]^{\mathrm{T}}$ the actuators' rotation angles, corresponding to the rotation of links connected to joints $Q_i$. The spider inverse kinematics defines the relationship mapping platform configuration $\mathbf{u}$ into $\mathbf{q}$, i.e.

$$\mathbf{q} = \mathbf{f}_{ik,s}(\mathbf{u}) \tag{3}$$

In the following, we summarize the main steps for the evaluation of $\mathbf{f}_{ik,s}$ function. According to the above definitions, the coordinates of the diamond vertices $A$, $B$, $C$, $D$ with respect to the platform frame $\mathcal{S}_p$ can be evaluated as a function of $\rho$ parameter only. Similarly, the coordinates of the spherical joints' centers $S_i$ connecting the moving platform to the legs (see Fig. 2c), can be evaluated in the mobile reference frame as a function of the $\rho$ parameter and are indicated as $\mathbf{r}_{S_i}^m$. Recalling the definition of $\mathbf{R}_m^b$ rotation matrix, and the position of $P$, defined by vector $\mathbf{r}_P$, we can easily evaluate the coordinates of the spherical joints with respect to the base frame: $\mathbf{r}_{S_i} = \mathbf{r}_P + \mathbf{R}_m^b \mathbf{r}_{S_i}^m$.

On the static upper base, the coordinates of the $Q_i$ points, $\mathbf{r}_{Qi}$ can be evaluated in the base frame with simple geometrical considerations, as a function of base parameters $L_b$ and $L_p$ indicated in Fig. 2b and Fig. 2c. We introduce eight auxiliary reference frames $\mathcal{S}_{qi}$, with origins in points $Q_i$, $z_i$ axes parallel to revolute joint axes, and $x_i$ axis on the $\langle x_b, y_b \rangle$ plane. The rotational matrix $\mathbf{R}_{q_i}^b$ represents the orientation of $\mathcal{S}_{qi}$ with respect to the base frame $\mathcal{S}_b$. We can then express the coordinates of $S_i$ points for such auxiliary reference frames

$$\mathbf{r}_{S_i} = [s_{p_{x_i}}, s_{p_{y_i}}, s_{p_{z_i}}]^T = \mathbf{R}_{q_i}^{b\ T} [\mathbf{r}_{S_i} - \mathbf{r}_{Qi}] .$$

This enables us to evaluate the components $q_i$ of the vector joint variables $q_i$ as:

$$q_i = 2 \arctan \left( \frac{s_{p_{y_i}} + \sqrt{s_{p_{x_i}}^2 + s_{p_{y_i}}^2 - w_i^2}}{w_i + s_{p_{x_i}}} \right)$$

with $w_i$ being an auxiliary variable defined as $w_i = \left(|\mathbf{r}_{S_i}| + L_1^2 - L_2^2\right)/(2L_1)$, This evaluation completes the inverse kinematic analysis.

For any configuration, the inverse differential kinematics provides a linear map between joint velocities and mobile platform velocities, i.e.:

$$\dot{\mathbf{q}} = \mathbf{J} \dot{\boldsymbol{\nu}} \tag{4}$$

The Jacobian matrix $\mathbf{J}$ is dependent on end effector configuration can be evaluated as

$$\mathbf{J} = \mathbf{J}_s \mathbf{J}_o \tag{5}$$

where $\mathbf{J}_s = \frac{\partial \mathbf{f}_{ik,s}}{\partial \mathbf{u}}$ is the actuator unit Jacobian, while $\mathbf{J}_o = \frac{\partial \mathbf{f}_{ik,o}}{\partial \boldsymbol{\nu}}$ is the end effector Jacobian.

The end effector Jacobian matrix $\mathbf{J}_o$ is $7 \times 7$ and can be evaluated as:

$$\mathbf{J}_o = \begin{bmatrix} \mathbf{I}_{3\times3} & skew(\mathbf{r}_{PP'}) & -\mathbf{R}_m^b \left[0,\ 0,\ -\frac{L_o}{2} \sin \frac{\delta}{2}\right]^{\mathrm{T}} \\ \mathbf{0}_{3\times3} & \mathbf{I}_{3\times3} & \mathbf{0}_{3\times1} \\ \mathbf{0}_{1\times3} & \mathbf{0}_{1\times3} & \frac{d\rho}{d\delta} \end{bmatrix} \tag{6}$$

where $skew(\mathbf{r}_{PP'})$ indicates the skew $3 \times 3$ skew matrix corresponding to the vector and $\frac{d\rho}{d\delta}$ consists in differentiating the inverse kinematic relationships defining $\rho$ parameter as a function of $\delta$.

The actuation unit Jacobian $\mathbf{J}_s = [\mathbf{J}_{s,1}^{\mathrm{T}}, \cdots \mathbf{J}_{s,8}^{\mathrm{T}}]^{\mathrm{T}}$ has dimensions $8 \times 7$ can be evaluated with considerations on leg kinematics. Each of its rows, $\mathbf{J}_{s,i}$ can be expressed as

$$\mathbf{J}_{s,i} = \mathbf{J}_{leg,i} \mathbf{J}_{p,i} \tag{7}$$

where $\mathbf{J}_{leg,i}$ is a $1 \times 3$ vector evaluated as

$$\mathbf{J}_{leg,i} = \frac{\mathbf{u}_{i,2}^{\mathrm{T}}}{(\mathbf{u}_{i,2} \times \mathbf{l}_{i,2}) \cdot \mathbf{u}_{i,2}} \tag{8}$$

while $\mathbf{J}_{p,i}$ is a $3 \times 7$ matrix evaluated as

$$\mathbf{J}_{p,i} = [\mathbf{I}_{3\times3} \quad \mathbf{S}_i \quad \mathbf{D}_i] \tag{9}$$

in which $\mathbf{S}_i$ is the $3\times3$ matrix relating the orientation angles' time derivatives to $U_i$ velocities, and $\mathbf{D}_i$ is a $3 \times 1$ vector that relates platform deformation velocity, evaluated as $\dot{\rho}$, to $U_i$ points' velocities. The details of differential kinematics evaluation for the actuation structure can be found in [30]. The device Jacobian matrix $\mathbf{J}$ allows to map forces and torques applied to the end effector to actuated joint torques. Indicating with $\boldsymbol{\tau}$ a $8 \times 1$ vector containing the torques applied by the motors, and with $\mathbf{f}$ the $7 \times 1$ vector of forces and torques applied by the end effector to the environment, by considering quasi-static conditions and by applying the Principle of Virtual Works it is immediate to verify that

$$\mathbf{f} = \mathbf{J}^{\mathrm{T}} \boldsymbol{\tau} \tag{10}$$

This relationship can be inverted to find, for a generic desired force vector at the end effector, the corresponding actuator torques. Since the device is redundant, it results that

$$\boldsymbol{\tau} = \left(\mathbf{J}^{\mathrm{T}}\right)^{+} \mathbf{f} + \mathcal{N}_{\mathcal{J}} \chi \tag{11}$$

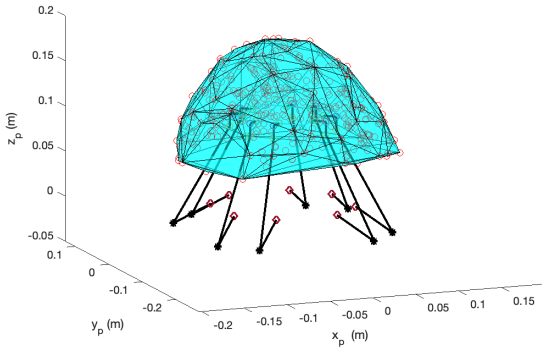


Fig. 3: Evaluation of end effector workspace. The cyan polyhedron contains the set of possible positions that can be reached by the origami vertex, red dots inside the polyhedron represent a subset of simulated configurations. Black lines represent spider structure legs in the reference configuration, corresponding to $x_p = y_p = 0$, $z_p = 0.1\,m$, $\alpha = \beta = \gamma = 0$ and in this case $\rho = L_p\sqrt{2}/2$.

where $^+$ indicates the pseudo-inverse operation, while $\mathcal{N}_\mathcal{J}$ is a matrix spanning $\mathbf{J}^{\mathrm{T}}$, that in a non-singular configuration has dimensions $8 \times 1$, while $\chi$ is an arbitrary value. Specifically, actuator torque vectors defined as $\boldsymbol{\tau}_0 = \mathcal{N}_\mathcal{J}\chi$ are torques that are balanced by structure constraint reactions and that do not produce any forces at the end effector.

## IV. Model-base Evaluation

### A. Workspace evaluation

The inverse kinematics relationships have been implemented in a Matlab script and adopted to evaluate the device workspace. Since the configuration space is 7-dimensional, to obtain a visual representation we performed different simulations selecting fixed values for the end effector orientation and vertex angle, and varying the vertex position. The workspace was evaluated by randomly selecting $10^6$ possible vertex positions in a $0.4{\times}0.4{\times}0.3\,m^3$ box around the device and checking for any of them if the inverse kinematics procedure provides a solution. The workspace is then approximated as the convex hull containing all the reachable positions. It is worth observing that this estimation tends to overestimate workspace volume since it can neglect local singularities or non-convexity, but at this stage of the analysis was considered a reasonable trade-off to verify if the structure is suitable for providing multidirectional haptic stimuli to hand palm. The workspace obtained with the dimensions of the prototype, that is, $L_p = 0.084\,m$, $L_b = 0.15\,m$, $L_1 = 0.051\,m$, $L_2 = 0.128\,m$, assuming $\alpha = \beta = \gamma = 0$ and $\rho = L_p\sqrt{2}/2$, as reported in Fig. 3. It is worth noticing that the workspace dimensions in the $x_p$, $y_p$, $z_p$ directions are $0.244$, $0.246$, and $0.13\,m$, respectively, and the workspace volume is $0.0041\,m^3$. Such values fit the device requirements for haptic applications: the origami vertex can reach any point of the hand palm of any adult human user.

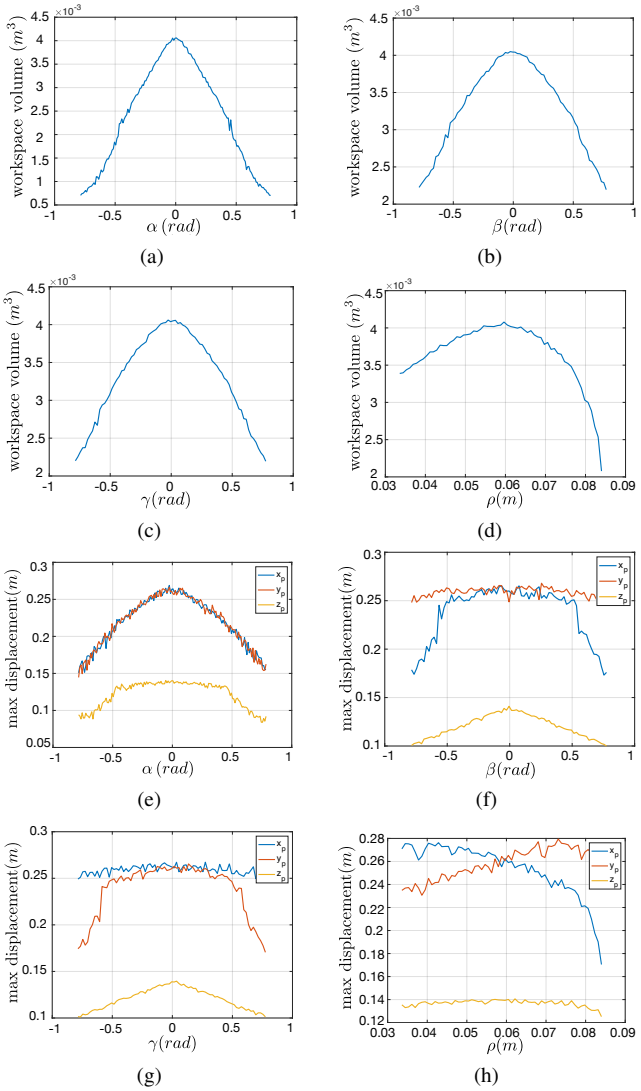


Fig. 4: Device workspace analysis. (a-d): volume of the set of device end effector positions that can be reached by origami vertex. (e-h): maximum displacements in the $x_p$, $y_p$, $z_p$ directions. Volume and maximum displacements are evaluated for different values of (a, e) $\alpha$ angle, (b, f) $\beta$ angle, (c, g) $\gamma$ angle, $(-\pi/4 < \alpha, \beta, \gamma < \pi/4)$, (d, h) $\rho$ parameter $(0.4L_p < \rho < L_p)$.

The set of possible positions that can be reached by the end-effector vertex has been evaluated for different values of the angles $\alpha$, $\beta$, and $\gamma$ (ranging between $-\pi/4$ and $\pi/4$), and for different values of $\rho$ parameter (ranging from $0.1L_p$ to $0.9\,L_p$). The results of this analysis are summarized in Fig. 4, in which the volume of the set of reachable end effector vertex positions and the maximum displacements in the $x_p$, $y_p$, $z_p$ are reported. It's worth noticing that both the volume and the maximum displacements decrease as the configuration moves from the reference. However, also at the boundaries of the considered variation, the displacements in the $x_p$ and $y_p$ directions are greater than $0.15\,m$, and in the $z_p$ direction are above $0.1\,m$, more than sufficient for haptic stimuli on the hand palm.

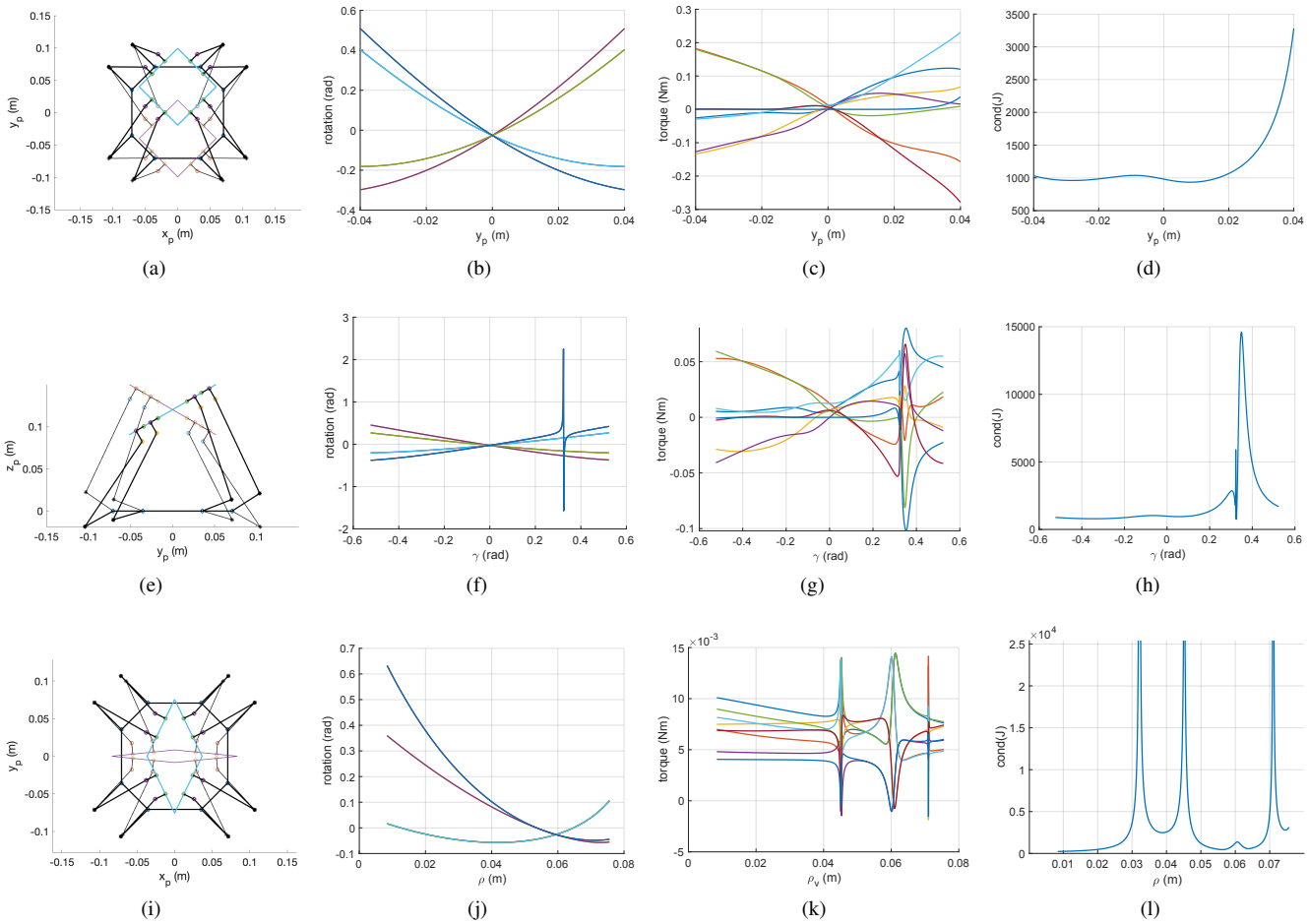


Fig. 5: Simulations of a subset of trajectories. (a, e, j) device initial (thin lines) and final (thick lines) configurations, (b, f, j) actuator angles, (c, g, k) actuator torques needed to apply a constant force with magnitude $1\,N$ in the vertical direction at the origami vertex, (d) device Jacobian condition number. First row: translation in the $y_p$ direction ($-0.04\,m < y_p < 0.04\,m$). Second row; rotation $\gamma$ along $x_p$ axis ($-\pi/6 < \gamma < \pi/6$). Third row: mobile platform reconfiguration parameter $\rho$ ($0.1L_p < \rho < 0.9L_p$).

### B. *Trajectory simulations*

The following analysis focused on the simulation of end effector trajectories and rotations. Simple straight trajectories, rotations along reference frame axes, and end effector deformation were evaluated. The results of a representative subset of simulations are reported in Fig. 5. For each trajectory, we reported: $(i)$ a scheme showing the initial and final configuration; $(ii)$ the results of inverse kinematic analysis in terms of $\mathbf{q}$ components as a function of system configuration; $(iii)$ for each configuration, the components of actuator torque vector $\boldsymbol{\tau}$ needed to balance a vertical force applied at the vertex of the end effector, with magnitude $1\,N$; $(iv)$ the condition number of Jacobian matrix. In parallel robot analysis, the Jacobian condition number is quite often used as an index to describe the closeness of a pose to singular configurations and more in general dexterity [31]. It can be noticed a discontinuity in the second simulation, by analyzing the specific case, it can be recognized that the discontinuity is motivated by angle representation, switching from $-\pi/2$ to $\pi/2$. Three local singularities can be identified in the last simulation, changing end-effector configuration while maintaining the other parameters fixed. Considering actuators able to apply a maximum torque of $0.3\,Nm$ as the ones adopted in the prototype, an external vertical force with magnitude $1\,N$ applied at the end effector can be sustained in all the configurations.

## V. Conclusion

In this paper we analyzed the performance of an origami-based haptic device for hand palm stimulation, actuated by a parallel robotic structure. The device has 8 actuators and 7-DoFs, so its redundant mechanical structure is versatile and capable of providing an extremely rich set of haptic stimuli. The availability of small-size actuators and additive manufacturing technology employing light, but resistant materials, led to a solution that can be either wearable or desktop based. In this paper, the mechanical structure was analytically investigated to evaluate device capabilities in terms of reachable configurations, and to set the basic inverse kinematics, differential kinematics and statics relationships necessary to implement effective position and impedance control strategies. Although the main focus of the presented work relies on the device analysis and simulation, we believe

that the results and methods could be of inspiration and contribute to the scientific knowledge and understanding of the problem related to the implementation of origami-inspired systems, in particular for haptic studies.

The mechanical design and simulation of the present device will inspire the research on hand-mounted haptic devices. The results of the analysis showed that the set of configurations that can be effectively reached and the forces that can be applied by the end-effector are more than sufficient for haptic stimuli on the hand palm. Moreover, the analysis showed important modeling reflections related to the determination of the force at the tip of the origami structure, in relation to the join variables. End effector trajectories and singularity issues have been investigated as well, with the aim of supporting the literature knowledge in future hardware developments (or tests) of the mechanical design. This work mainly aims at better exploring the analysis of the proposed device. We believe that the presented analysis can support research on the design of origami-like platforms, providing a diverse interpretation to address the problem of presenting varied cutaneous cues to the user, to provide a more complete haptic experience. Future developments of this work will further investigate device control and assess the device properties with specific quantitative laboratory tests and user studies. From the design point of view, the combination of a rigid parallel robotic structure for the actuation with an origami structure for the application of haptic stimuli can be further developed exploiting soft structures with continuous deformation.

## REFERENCES


[1] C. Pacchierotti, S. Sinclair, M. Solazzi, A. Frisoli, V. Hayward, and D. Prattichizzo, "Wearable haptic systems for the fingertip and the hand: taxonomy, review, and perspectives," *IEEE Trans. Haptics*, vol. 10, no. 4, pp. 580–600, 2017.

[2] J. J. Fleck, Z. A. Zook, J. P. Clark, D. J. Preston, D. J. Lipomi, C. Pacchierotti, and M. K. O'Malley, "Wearable multi-sensory haptic devices," *Nature Reviews Bioengineering*, pp. 1–15, 2025.

[3] C. Pacchierotti and D. Prattichizzo, "Cutaneous/tactile haptic feedback in robotic teleoperation: Motivation, survey, and perspectives," *IEEE Trans. Robotics*, vol. 40, pp. 978–998, 2023.

[4] D. Torielli, L. Franco, M. Pozzi, L. Muratore, M. Malvezzi, N. Tsagarakis, and D. Prattichizzo, "Wearable haptics for a marionette-inspired teleoperation of highly redundant robotic systems," in *2024 IEEE International Conference on Robotics and Automation (ICRA)*. IEEE, 2024, pp. 15 670–15 676.

[5] P. Kourtesis, F. Argelaguet, S. Vizcay, M. Marchal, and C. Pacchierotti, "Electrotactile feedback applications for hand and arm interactions: A systematic review, meta-analysis, and future directions," *IEEE Trans. haptics*, vol. 15, no. 3, pp. 479–496, 2022.

[6] J. Park, Y. Oh, and H. Z. Tan, "Effect of cutaneous feedback on the perceived hardness of a virtual object," *IEEE Trans. haptics*, vol. 11, no. 4, pp. 518–530, 2018.

[7] B. Hannaford and A. M. Okamura, "Haptics," *Springer handbook of robotics*, pp. 1063–1084, 2016.

[8] D. Wolf, M. Rietzler, L. Hnatek, and E. Rukzio, "Face/on: Multi-modal haptic feedback for head-mounted displays in virtual reality," *IEEE Trans. Visualization and Computer Graphics*, vol. 25, no. 11, pp. 3169–3177, 2019.

[9] L. Kuang, M. Aggravi, P. R. Giordano, and C. Pacchierotti, "Wearable cutaneous device for applying position/location haptic feedback in navigation applications," in *Proc. IEEE Haptics Symposium (HAPTICS)*, 2022, pp. 1–6.

[10] Y. Yamazaki and S. Hasegawa, "Navigation method enhancing music listening experience by stimulating both neck sides with modulated musical vibration," *IEEE Trans. Haptics*, vol. 16, no. 2, pp. 228–239, 2023.

[11] S. Schaack, G. Chernyshov, K. Ragozin, B. Tag, R. Peiris, and K. Kunze, "Haptic collar: Vibrotactile feedback around the neck for guidance applications," in *Proceedings of the 10th Augmented Human International Conference 2019*, 2019, pp. 1–4.

[12] J. Kim, H. Kim, C. Park, and S. Choi, "Human recognition performance of simple spatial vibrotactile patterns on the torso," in *2023 IEEE World Haptics Conference (WHC)*. IEEE, 2023, pp. 20–27.

[13] T. Moriyama and H. Kajimoto, "Wearable haptic device presenting sensations of fingertips to the forearm," *IEEE Trans. Haptics*, vol. 15, no. 1, pp. 91–96, 2022.

[14] F. Chinello, C. Pacchierotti, J. Bimbo, N. G. Tsagarakis, and D. Prattichizzo, "Design and evaluation of a wearable skin stretch device for haptic guidance," *IEEE Robotics and Automation Letters*, vol. 3, no. 1, pp. 524–531, 2017.

[15] F. Berton, F. Grzeskowiak, A. Bonneau, A. Jovane, M. Aggravi, L. Hoyet, A.-H. Olivier, C. Pacchierotti, and J. Pettre, "Crowd navigation in vr: exploring haptic rendering of collisions," *IEEE Trans. Visualization and Computer Graphics*, vol. 28, no. 7, pp. 2589–2601, 2020.

[16] D. K. Chen, I. A. Anderson, C. G. Walker, and T. F. Besier, "Lower extremity lateral skin stretch perception for haptic feedback," *IEEE Trans. haptics*, vol. 9, no. 1, pp. 62–68, 2016.

[17] M. Aggravi, D. A. Estima, A. Krupa, S. Misra, and C. Pacchierotti, "Haptic teleoperation of flexible needles combining 3d ultrasound guidance and needle tip force feedback," *IEEE Robotics and Automation Letters*, vol. 6, no. 3, pp. 4859–4866, 2021.

[18] M. A. Cabrera, J. Tirado, J. Heredia, and D. Tsetserukou, "Linkglide-s: A wearable multi-contact tactile display aimed at rendering object softness at the palm with impedance control in vr and telemanipulation," pp. 647–652, 2022.

[19] D. Trinitatova and D. Tsetserukou, "Deltatouch: a 3d haptic display for delivering multimodal tactile stimuli at the palm," in *Proc. IEEE World Haptics Conference (WHC)*, 2019, pp. 73–78.

[20] K. Iiyoshi, S. Khazaaleh, A. S. Dalaq, M. F. Daqaq, G. Korres, and M. Eid, "Origami-based haptic syringe for local anesthesia simulator," *IEEE Trans. Haptics*, vol. 17, no. 1, pp. 39–44, 2024.

[21] L. Kuang, M. Malvezzi, D. Prattichizzo, P. R. Giordano, F. Chinello, and C. Pacchierotti, "The hapticspider: a 7-dof wearable device for cutaneous interaction with the palm," in *International Conference on Human Haptic Sensing and Touch Enabled Computer Applications*. Springer, 2024, pp. 285–292.

[22] M. Mangalam, S. Oruganti, G. Buckingham, and C. W. Borst, "Enhancing hand-object interactions in virtual reality for precision manual tasks," *Virtual Reality*, vol. 28, no. 4, p. 166, 2024.

[23] F. H. Giraud, S. Joshi, and J. Paik, "Haptigami: A fingertip haptic interface with vibrotactile and 3-dof cutaneous force feedback," *IEEE Trans. Haptics*, vol. 15, no. 1, pp. 131–141, 2021.

[24] A. Villani, M. Dragusanu, D. Prattichizzo, and M. Malvezzi, "Validation and usability assessment of the hapticpalm, a wearable device for hand palm force feedback," in *Proc. IEEE Haptics Symposium*, 2024, pp. 372–378.

[25] M. Dragusanu, A. Villani, D. Prattichizzo, and M. Malvezzi, "Design of a wearable haptic device for hand palm cutaneous feedback," *Frontiers in Robotics and AI*, vol. 8, p. 706627, 2021.

[26] X. Yin, J. Wu, J. Yan, Y. Lu, and Y. Song, "Design of an origami-inspired haptic interface for catheter interventional surgery," *IEEE Sensors Journal*, vol. 24, no. 5, pp. 6867–6879, 2024.

[27] G. Korres, K. Iiyoshi, and M. Eid, "Origami-inspired vibrotactile actuator (orivib): Design and characterization," *IEEE Trans. Haptics*, vol. 17, no. 3, pp. 496–502, 2023.

[28] S. R. Williams, J. M. Suchoski, Z. Chua, and A. M. Okamura, "A 4-degree-of-freedom parallel origami haptic device for normal, shear, and torsion feedback," *IEEE Robotics and Automation Letters*, vol. 7, no. 2, pp. 3310–3317, 2022.

[29] H. Ren, *Wearable Origami Rendering Mechanism Towards Haptic Illusion*. Springer, 2023, pp. 379–399.

[30] P. Lambert and J. L. Herder, "A 7-dof redundantly actuated parallel haptic device combining 6-dof manipulation and 1-dof grasping," *Mechanism and Machine Theory*, vol. 134, pp. 349–364, 2019.

[31] A. Chandrashekhar and G. S. Babu, "Jacobian matrix and kinematic analysis of the parallel robots: A survey." *IUP Journal of Mechanical Engineering*, vol. 8, no. 3, 2015.